Journal of Engineering and Science Research 6 (5): 12-28, 2022
e-ISSN: 2289-7127

DOI: 10.26666/rmp.jesr.2022.5.3

Numerical Assessment of Vertical Axis Tidal Turbine Performances in Shallow Water

Muhammad Wafiuddin Abd Rahim[a], Anas Abdul Rahman[a], Mohd Asari Bakri[a], Ayu Abdul-Rahman[b], Muhammad Izham Ismail[c], Nasrul Amri Mohd Amin[a], Mohd Shukry Abdul Majid[a]

[a]Faculty of Mechanical Engineering Technology, Universiti Malaysia Perlis, Pauh Putra Main Campus, 02600 Perlis, Malaysia.

[b]Department of Mathematics and Statistics, School of Quantitative Sciences, Universiti Utara Malaysia, 06010 UUM, Sintok, Kedah, Malaysia

[c]Faculty of Applied and Human Sciences, Universiti Malaysia Perlis (UniMAP), Pauh Putra Main Campus, 02600 Arau, Perlis Malaysia

Received: 10 August 2022; Revised: 08 September 2022; Accepted: 12 October 2022; Published: 30 October 2022

Abstract: Although blessed with plenty of natural resources, Malaysia has now begun transitioning away from them towards renewable energy alternatives. This is evidenced by various initiatives and plans made towards reducing dependency on hydrocarbons, such as a pledge to "become a carbon neutral country by 2050 as outlined in 12th Malaysia Plan. Among the green energy that can be considered, explored, and focused on by Malaysia is marine renewable energy, such as tidal, since the country is surrounded by large oceans. Nonetheless, there is currently insufficient data regarding the behaviour of the flow when passing through the devices downstream, especially in shallow water applications. Thus, this paper aims to highlight on the turbulence wake characteristics, and also to analyse the behaviour of wake produced by the vertical axis tidal turbine (VATT) in harnessing tidal energy at shallow water application, specifically further downstream of the device. Comparison will be made against the horizontal axis tidal turbine (HATT) to highlight their differences. Numerical analysis using the CFD method is used to analyse the model of turbines, which is represented by cylindrical and disc geometries. The simulation is evaluated in terms of the wake characteristic for both single and array configurations of the turbine. From a previous study, it has been demonstrated that the wake distance has a significant influence on the performance of tidal devices on the subsequent rows. Hence, this statement is examined in this research work to verify its validity for vertical axis tidal turbines.

Keywords: *Horizontal axis tidal turbine, Hypothetical actuator cylinder, Hypothetical actuator disc, Turbulence wake, Marine renewable energy*

INTRODUCTION

Malaysia is known as one of the countries that are rich in natural resources such as plantation, forestry, bauxite, oil and gas. All of these are categorized as non-renewable energy which means they will deplete in the future. For example oil and gas sector produced 74,400 barrels of oil production per day [1], and based on the 1998-2010 trend, the reserve's oil will probably deplete by 2035 [2]. Therefore, the solution to this problem is by using renewable energy such as tidal current, wind energy, and solar. The interest of this paper is towards the utilisation of tidal current since Malaysia is surrounded by a large bodies of water. There is various kinds of technology that exists to harness this type of energy. Europe is currently at the forefront in regards to harnessing energy from the ocean, either from wave or

Corresponding Author: Anas Abdul Rahman, Mechanical Engineering Program, Faculty of Mechanical Engineering Technology, Universiti Malaysia Perlis, Pauh Putra Main Campus, 02600 Arau, Perlis, Malaysia, anasrahman@unimap.edu.my

tidal currents [3]. **Figure 1** shows the general process of how the tidal turbine works.

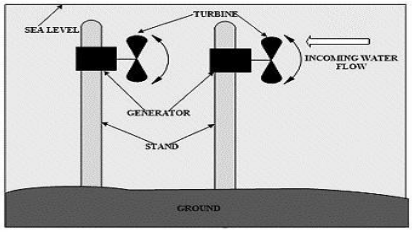

Figure 1: Tidal stream method to harness energy from the energy [4]

To know whether Malaysia is ready for the implementation of this technology, research needs to be done to determine the kind of turbines that are suitable for deployment. Even though Malaysia is covered mostly with open water, the depth of its seas is not deep enough for common tidal devices to be mounted under the seabed. Notably, the maximum depth of Malaysia's open channel is about 60 meters [2],[5]. Thus, the selection of types of tidal turbines needs to be based on Malaysia's geographical aspects. From the previous study conducted by Hoe [6], a preliminary study on the Horizontal Axis Tidal Turbine (HATT) specifically on the array configuration had been done.

The research was focused to identify the behaviour of HATT at Malaysia's open water channel in terms of the velocity contour, wake generation, and configuration of various arrays layout. Although results from his study showed an excellent output, it is important to remember that the depth of the Malaysian ocean is not the same as in Europe. Hence, a lot of things need to be considered such as the top and bottom clearance since the HATT blades would be mounted on the horizontal axis. Notably, another alternative is to utilise a Vertical Axis Tidal Turbine (VATT) instead of HATT. Thus, the purpose of this paper is to analyse, validate and compare the two different types of tidal turbines in terms of wake generation and array configuration to determine which device are better suited for deployment in Malaysia's open water. Figure 2 shows an example of an existing model of tidal turbines that are used for deep water applications.

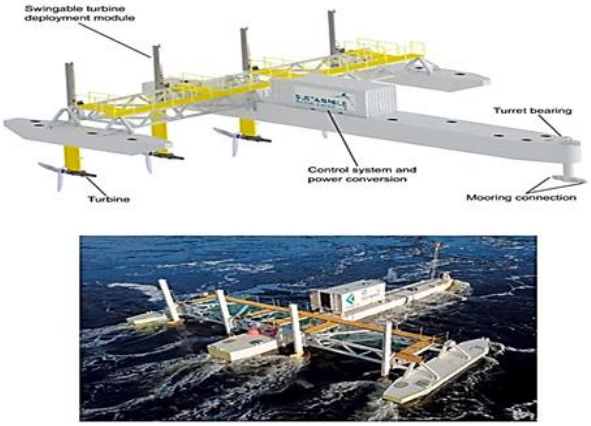

Figure 2: The design of turbine modular tidal converter [7]

NUMERICAL ANALYSIS

Numerical analysis is the method of using the Computational Fluid Dynamics (CFD) approach to understand the behaviour of the turbines under a certain parameter. It involves the process of simulating the flow behind a tidal stream turbine which poses several challenges, especially in the near-wake region where the region is so close to the turbines [8]. As shown in Table 1, various CFD methods can be used to conduct a numerical investigation. Notably, the hypothetical actuator cylinder model was employed in this study to represent the vertical axis tidal turbine (VATT) since this method can reduce computational cost. Note that instead of computing the source term for the actuator cylinder/disc model to function, cylindrical and circular objects are being used to represent the device. Notably, the CFD method can be analysed by using software such as ANSYS, Telemac 3D, and EllipSys3D.

Table 1: Types of CFD approaches

Method	Description
Actuator Cylinder (AC) used in this research 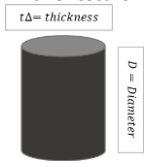	• Similar to the actuator disc shape with different height and axis. • Assume steady flow conditions, neglect the effect that caused by the discrete blades and swirl effect on the turbine [6]. • Fast simulation [9].
Blade Element Momentum (BEM) [10] [11] 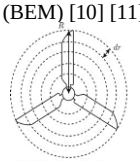	• A method which negligible the effect of blockage on rotor performance [11]. • Combination between CFD and BEM theory for modification of momentums equation [10].

Actuator Line Model (ALM) [12] 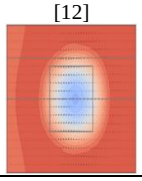	• Combination of classic blade element theory with the Navier-Stoke [12]. • Treat turbine blades as lines of blade or as the actuator line elements [12].
Full Scale Model [13] 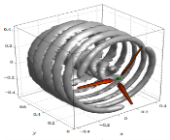	• Very complex meshing due to large scale parameters [13]. • All geometry of the rotor is placed inside computational domain.

Reynold's Average Navier Stoke (RANS) Approach

Reynold's Average Navier Stoke is an averaged equation of motion for fluid flow. The equation is used to describe any problems that involve fluid flow especially turbulence flows. Simulation using the CFD method will be used along with the RANS approach to do the simulation of the actuator cylinder. RANS approach was chosen because this method requires low computational cost and less time-consuming when doing the simulation compare to other approaches such as large eddy simulation (LES) and direct numerical simulations (DNS) [14].

$$\rho\frac{\partial \boldsymbol{u}}{\partial t}+\rho\boldsymbol{u}.\nabla\boldsymbol{u}=-\nabla p+\mu\nabla^2\boldsymbol{u}-\nabla.(\rho\boldsymbol{u}'\boldsymbol{u}')+S_u \quad (1)$$

where u is the mean velocity, $\boldsymbol{u}'$ is the fluctuating velocity, p is pressure, μ is dynamic viscosity, and S_u stand for momentum. The final equation will contain the Reynolds stress $\rho\boldsymbol{u}'\boldsymbol{u}'$ tensor on the right side [14]. It represents the turbulent fluctuations in the flow, and are defined as follows for incompressible flows:

$$\rho\boldsymbol{u}'\boldsymbol{u}'=\overline{\overline{T_R}}=-\frac{2}{3}k\rho\boldsymbol{I}+\mu_T(\nabla\boldsymbol{u}+(\nabla\boldsymbol{u}^T)) \quad (2)$$

where $k=(\boldsymbol{u}'.\boldsymbol{u}')/2$ is for turbulent kinetic energy and μ_T is dynamic eddy viscosity. These equations are then substituted for k and turbulent frequency ω:

$$\rho\frac{\partial \boldsymbol{u}}{\partial t}+\rho\boldsymbol{u}.\nabla k=\nabla.\left((\mu+\sigma^*\mu_T)\nabla k\right)+\overline{\overline{T_R}}.\nabla\boldsymbol{u}-\rho\beta^*k\omega+S_k \quad (3)$$

$$\rho\frac{\partial \boldsymbol{u}}{\partial t}+\rho\boldsymbol{u}.\nabla\omega=\nabla.\left((\mu+\sigma\mu_T)\nabla\omega\right)+\alpha(\frac{\omega}{k})\overline{\overline{T_R}}.\nabla\boldsymbol{u}-\rho\beta\omega^2+S_\omega \quad (4)$$

where $\sigma=0.5, \sigma^*=0.5, \beta^*=0.09$, and $\alpha=5/9$ [14]. S_k and S_ω represent the additional parameters that are not included or presented in the standard $k-\omega$ RANS model, but it is included here to show the presence of the hypothetical actuator cylinder.

METHODOLOGY

For the cylindrical object (i.e., hypothetical actuator cylinder), the geometry was created by using CATIA. Meanwhile, the domain representing the open channel was created inside ANSYS. The use of two software to create the geometry is because when using CATIA, the axis of the domain cannot be assembled with the cylindrical object. Therefore, upon creating the geometry, the subsequent simulation procedure took place inside ANSYS Workbench.

Single Turbine Study

For a single turbine study, the parameters of the domain and device were extracted from a study conducted by Hoe [6]. Only a few parameters were altered related to the geometry of the turbine. The previous study used a circular object (i.e., hypothetical actuator disc) to represent HATT while the current study would be employing a cylindrical object (i.e. hypothetical cylinder) to represent VATT.**Error! Reference source not found.** highlights a comparison between the parameters used in this current work and previous studies by Hoe [6]. Meanwhile, the domain for the single turbine remained the same as used by Hoe [6] and the validation of the parameter is also shown i**Error! Reference source not found.**. Since there is a cylindrical object inside the domain, whenever fluid passes through the object, the velocity is reduced due to a phenomenon called the blockage factor. Therefore, the blockage factor was calculated to ensure there is no addition in acceleration from the fluid inside the domain. Additionally, Figure 3 shows the schematic diagram of the domain used in this study based on the parameters highlighted in Table 2.

Table 3: Validation of different numerical modelling for a single turbine

Parameters	Numerical (HATT model by Hoe [6])	Numerical (VATT model)
Disc/Cylinder diameter	5 m	5 m
Disc thickness/Cylinder height	1 m	5 m
Blockage ratio	0.0191	0.0191
Depth of domain	30 m (from literature)	30 m
Width of domain	34 m (calculation by Hoe)	34 m
Length of domain	250 m (calculation by Hoe)	250 m
Disc/Cylinder positioning	62.5 m from inlet	62.5 m from inlet

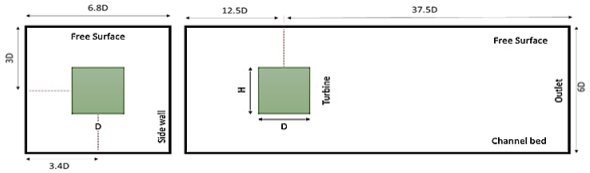

Figure 3: Schematic diagram that illustrates the dimension of the domain for a single turbine study (use in this research)

Dual turbine and Array Turbines Study

Array study in this research is focused on the layouts of the lateral spacing (LS), longitudinal spacing (LGS), and staggered array. For LS and LGS, three different dimensions of spacing were used. For LS, the simulation was done in 0.5D,1.0D, and 1.5D. Next, for LGS, the simulation was done in 2.5D, 3.0D, and 3.5D. Each spacing is expected to develop a different velocity contour across the domain. Domain parameters for the array turbine study are quite similar to the one used for the single turbine study as illustrated in Figure 4. Notably, just like with a single turbine study, the domain parameters that was employed for the array study would be the same as the one adopted by Hoe. However, the blockage ratio used in the array study is different than the one for the single turbine study. In the array study, a blockage ratio of 0.0116 was used for both two and three cylinders. Additionally, the width of the domain for the single turbine is 34 meters, while for the array study the width was set to 56 meters to ensure the turbines will have adequate spacing inside the domain, while other parameters remain unchanged.

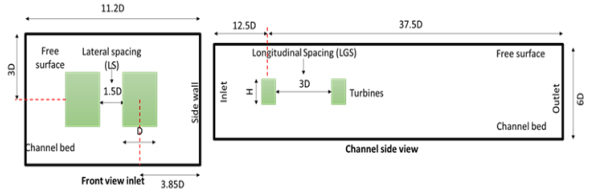

Figure 4: Schematic diagram that illustrates the dimension of the domain for array turbine study (use in this technical paper)

Meshing Configuration

Meshing for array turbine study will be different from single turbine study. For the array study, only localised mesh was used. The reason for using localised meshing was because the results in single turbine study indicates better output when compared to globalised meshing as illustrated in Figure 5. Therefore, the results presented in this paper will be based on the output of models that were imposed with localised meshing. Since the domain parameters have been changed, some parameters in the meshing setup needed to be changed as well. As the domain width for the array setup is increased (56 meters), the element size for the body were also changed as well from 2.0 meters (single device) to 2.5 meters (multiple devices). The element size for face meshing and edge meshing remains the same as in the single turbine study, which is 0.1 meter.

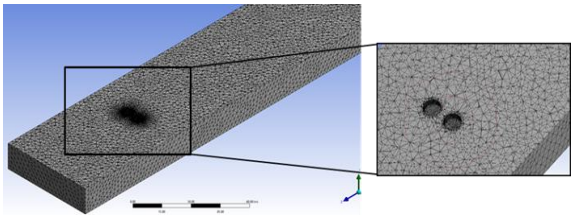

Figure 5: Localised body meshing for LS0.5D with a zoom image at the turbine area

RESULT AND DISCUSSION

Validation Between HATT and VATT for Single Turbine

Validation of Velocity Contour

Figure 6 shows the result of a single turbine simulation for VATT and HATT. The differences in terms of the shape of the turbine play a major influence on the velocity contour to spread along the domain. The blue region area which is having the lowest velocity for VATT is smaller compared to the blue region area for HATT. The evaluation and the observation of the velocity contour between VATT and HATT had been observed by comparing the wake recovery region along the domain. Next is the evaluation in terms of the comparison between VATT and HATT in shallow water application against statistical data for modelled, numerical for HATT and experimental data need to be extracted and compared. Numerical data for HATT are extracted from Hoe [6], modelled and experimental data are from Harrison et al.[15]. The '+' marker in black color represents the experimental data, the blue and red line represent modelled and HATT data respectively and the green scatter is represented the VATT data.

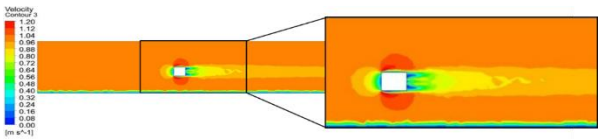

(a)

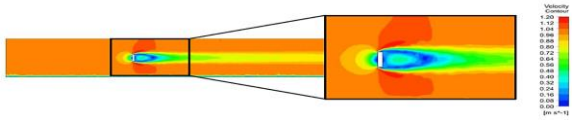

(b)

Figure 6: Horizontal velocity contour of y-plane slices for single turbine: (a) VATT (b) HATT

Validation of Normalized Velocity and Normalized Turbulence Intensity for Single Turbine

For normalized velocity as shown in Figure 7, it can be concluded that a single turbine for VATT has faster wake recovery at 7D and 11D downstream meanwhile for HATT, the wake recovered faster at 4D and 20D downstream. Additionally, as shown in Figure 8 for normalised turbulence intensity, both numerical results fall on the left-hand side of the data. According to Hoe [6], this occurs due to the domain being set up to 2-meter element size and no details refinement at the critical zone of the domain. It will affect the homogeneity of the flow in HATT and this factor may affect VATT also to reach the equilibrium state to represent the actual turbulence flow in the experiment conducted by Harrison et al. [15]. But still the numerical (VATT and HATT) turbulence intensity can be considered valid because the gap between numerical and experimental continue to decrease at the far wake region.

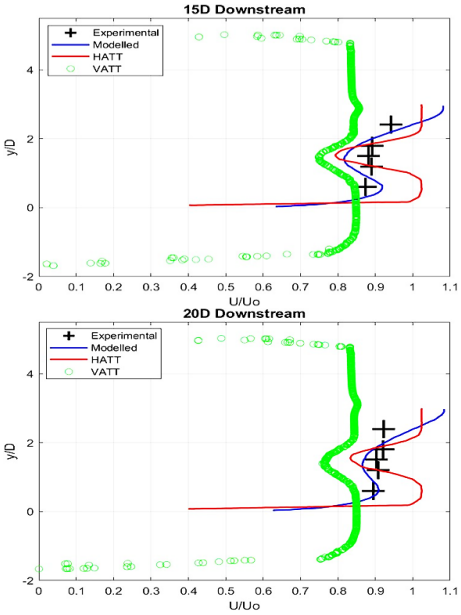

Figure 7: Normalized Velocity for VATT, HATT by [6], and experimental by [15] for single turbine study

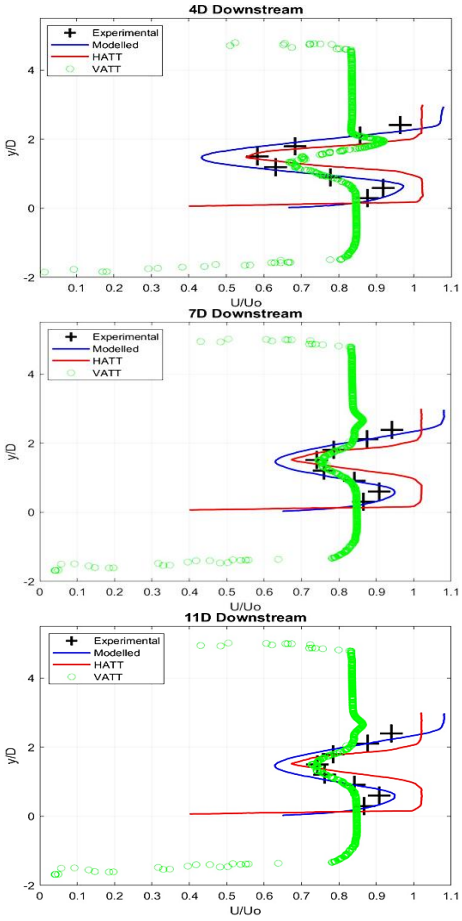

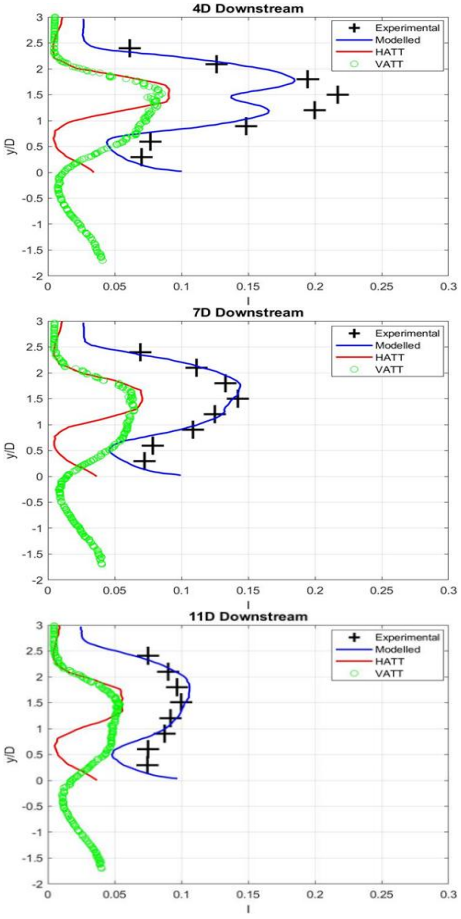

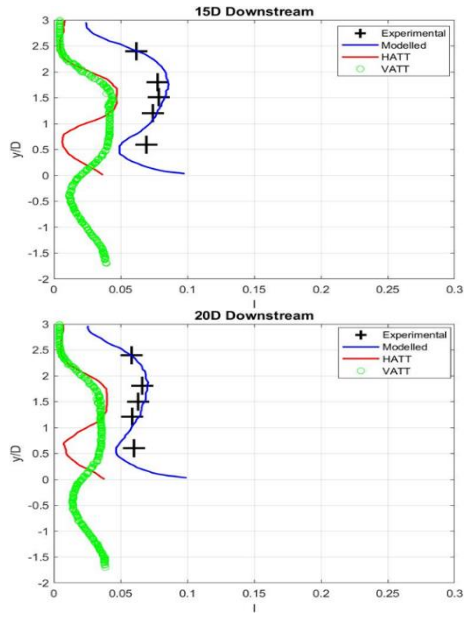

Figure 8: Normalized turbulence intensity for VATT, HATT by [6], and experimental by [15] for single turbine study

Table 4: Percentage of deviation data between VATT and experimental for normalized velocity

Single turbine downstream distances	**Vertical Tidal Turbine VS Experimental**				
	4D	7D	11D	15D	20D
Percentage of deviation (%)	20.69	1.35	1.33	14.77	13.07

From Table 4, the deviation difference between VATT and experimental is about 20.69%. But as the downstream increases to 7D and 11D, the deviation begins to reduce to the left-hand side of the data with only 1.35% and 1.33% respectively. Despite their difference in the variation of the normalized velocity, both numerical results for VATT and HATT show less deviation in terms of the normalized turbulence intensity. Additionally, Table 5 shows that the variation of the turbulence intensity of VATT across the far wake is decreasing. At 4D downstream, the deviation between the experimental is 69.57% and when it reached the far wake at 20D the deviation was only 23.53% error.

Table 5: Percentage of deviation data between VATT and experimental for normalized turbulence velocity

Single turbine downstream distances	**Vertical Tidal Turbine VS Experimental**				
	4D	7D	11D	15D	20D
Percentage of deviation (%)	69.57	50.00	41.00	25.00	23.53

Validation Between HATT and VATT for Dual Turbine

Validation of Velocity Contour

For dual turbine simulations, all the simulations were done by using localized meshing with soft behavior option as discussed in the single turbine simulation section. Dual turbines are divided into three types of lateral spacing simulation; LS0.5D, LS1.0D and LS1.5D. Having the same setting for the simulations as a single turbine configuration, only the lateral spacing of two turbines is distinct. The simulation result for VATT in Figure 9 shows that as the lateral spacing increases from 0.5D to 1.5D, the wider the stream flow spread away from each other across the domain. The wake generated is also affected by the lateral spacing. As the lateral spacing increases, the shorter the time for the stream to become uniform at the wake region and the lower the chances for the flow to merge at the wake region. By comparing the result for HATT and VATT regarding their differences in lateral spacing, all the results indicate that VATT does have a faster wake recovery compared to HATT.

The velocity of HATT for dual turbine takes a longer period to recover after it passes through the turbine by observing the blue region area of each LS for HATT. For both VATT and HATT, the wake recovery for LS0.5D is the slowest among the other LS. This occurs due to small spacing that causes the kinetic energy of the fluid unable to flow or pass thru the small channel. The small channel will lead to the dissipation of excess energy to the side of the cylinder and the disc as well. Velocity passing the cylinder geometry are concentrated or dispersed at the left and right-hand side of the cylinder due to the curvature effects that had been discussed in the single turbine section. For this case, it involved two cylinders and when incoming velocity reaches the curved surface of the cylinder, both are being dispersed simultaneously and less turbulence mixing occurs in near wake region.

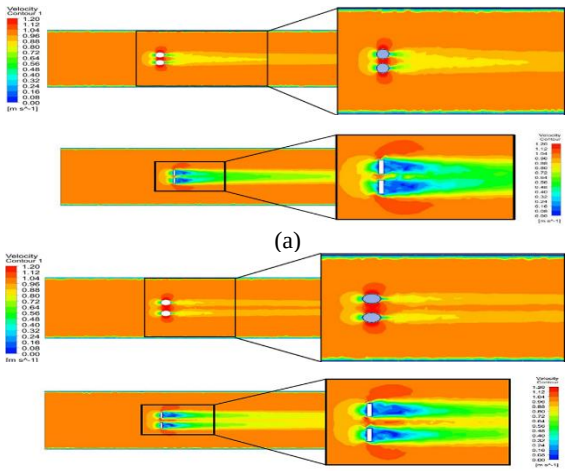

(a)

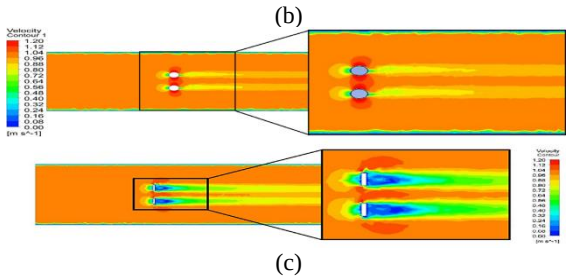

Figure 9: Comparison of velocity contour between VATT (cylinder shape) and HATT (disc shape) in: (a) LS0.5D (b) LS1.0D (c) LS1.5D.

Validation of Normalized Velocity for Dual Turbines

In dual turbines, the normalized velocity is done by comparing the numerical results between VATT and HATT. The data being extracted are from 5D, 7D, 9D, and 25D downstream. The evaluation of the graph data is made by comparing similar downstream but in different lateral spacing (LS0.5D, LS1.0D and LS1.5D) and the validation is made between VATT, HATT and experimental. As illustrated in Figure 10 until Figure 13, the normalized velocity data for the numerical results of VATT and HATT fall on the left-hand side of the graph. Throughout the normalized velocity result, it shows that the deviation between both numerical results (VATT and HATT) and the experimental are decreasing as the downstream and the lateral spacing increase. Despite the decreases in the deviation being in good agreement, there is some unavoidable error that might be the factors that affect the data such as parallax error during measurement by using a velocimeter [6].

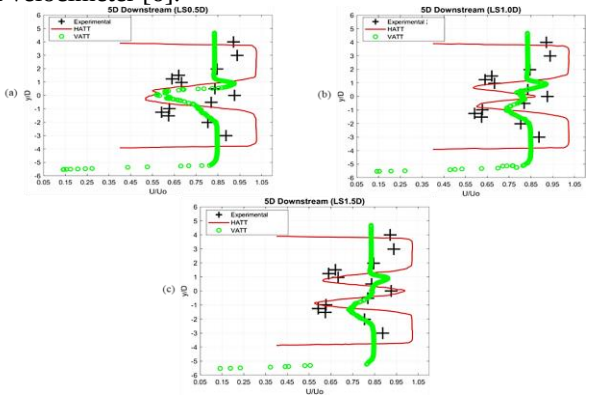

Figure 10: Comparison of LS for HATT and VATT in terms of normalized velocity at mid-channel depth for 5D downstream: (a) LS0.5D, (b) LS1.0D, (c) LS1.5D.

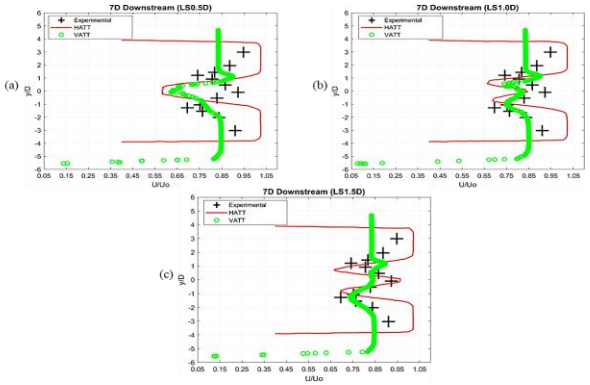

Figure 11: Comparison of LS for HATT and VATT in terms of normalized velocity at mid-channel depth for 7D downstream: (a) LS0.5D, (b) LS1.0D, (c) LS1.5D.

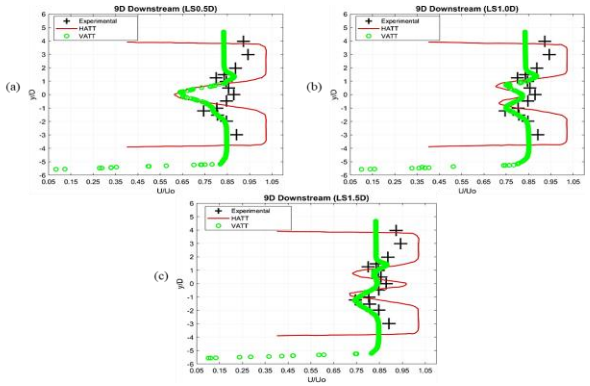

Figure 12: Comparison of LS for HATT and VATT in terms of normalized velocity at mid-channel depth for 9D downstream: (a) LS0.5D, (b) LS1.0D, (c) LS1.5D.

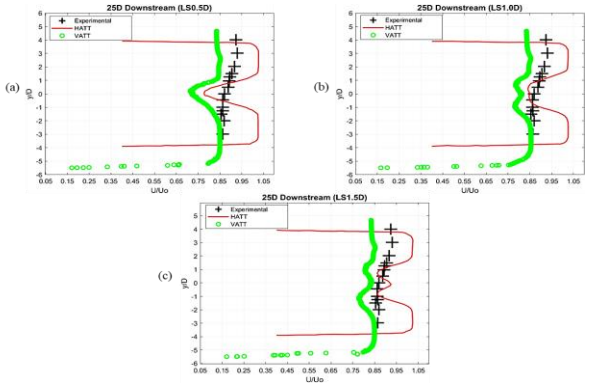

Figure 13: Comparison of LS for HATT and VATT in terms of normalized velocity at mid-channel depth for 25D downstream: (a) LS0.5D, (b) LS1.0D, (c) LS1.5D.

On the other hand,

Table 6 and Table 7 show that at LS0.5D, s comparison between VATT and HATT against the experimental data has a larger deviation with 37.50% and 35.23% error at 5D downstream. The deviation of LS0.5D along 7D, 9D, and 25D still shows a deviation that more than 10% error. Thus, the lateral spacing of 0.5D in all downstream can be classified as inappropriate spacing because the spacing gave poor

results with a larger deviation from the experimental data.

Table 6: Percentage of deviation data between VATT and experimental

Dual Turbines		Vertical Tidal Turbine VS Experimental			
	Downstream	**5D**	**7D**	**9D**	**25D**
Percentage of deviation	LS 0.5D	37.50%	34.41%	27.27%	16.09%
	LS 1.0D	12.50%	9.68%	4.55%	4.49%
	LS 1.5D	3.41%	11.83%	3.22%	2.30%

Table 7: Percentage of deviation data between HATT and experimental

Dual Turbines		Horizontal Tidal Turbine VS Experimental			
	Downstream	**5D**	**7D**	**9D**	**25D**
Percentage of deviation	LS 0.5D	35.23%	37.63%	31.82%	10.75%
	LS 1.0D	2.27%	8.60%	5.68%	2.63%
	LS 1.5D	9.09%	3.23%	9.09%	5.40%

However, as the lateral spacing increases from LS1.0D to LS1.5D along the 5D, 7D, 9D and 25D, the deviation starts to decrease and the gap between the numerical results and the experimental are closer to each other. The deviation between numerical results for VATT with experimental at LS1.0D and LS1.5D are 12.50% and 3.41% respectively at 5D downstream. By comparison of the deviation between numerical results and experimental, the numerical results for HATT had the least deviation compared to VATT. This occurs because the experimental data by Harrison et al. only were based on HATT design, and not for VATT turbine. For future recommendation, the validation between numerical results for VATT and experimental data involving the VATT for small-scale turbine can be made. As highlighted in

Table 8, the difference of error between the numerical results of VATT and HATT is less despite the geometrical difference and the axis of the turbine.

Table 8: Deviation difference between VATT and HATT

Dual Turbines		Vertical Tidal Turbine and Horizontal Tidal Turbine			
	Downstream	**5D**	**7D**	**9D**	**25D**
Percentage of deviation	LS 0.5D	2.27%	3.22%	4.55%	4.60%
	LS 1.0D	10.23%	1.08%	1.13%	1.04%
	LS 1.5D	5.68%	8.60%	5.87%	1.26%

Validation Between HATT and VATT for Array Configurations (Dual-Frontal Staggered Array)

Validation of Velocity Contour

For dual frontal staggered arrays simulations, three types of lateral spacing were examined - LS0.5D, LS1.0D, and LS1.5D, which is similar to dual turbines. The difference for dual frontal staggered array, however, is the addition of a cylinder placed directly behind the dual frontal cylinder. The interest in adding a cylinder at the longitudinal spacing is to observe and identify the behavior of the array configurations of three cylinders inside a domain. The simulations were done in three different longitudinal spacing (LGS2.5, LGS3.0D, and LGS3.5D). Figure 14 shows the comparison of LS0.5D in LGS2.5D, LGS3.0D, and LGS3.5D for VATT and HATT. At LGS2.5D both velocity contours of VATT and HATT gave the slowest wake recovery as demonstrated by the yellow and green region along the downstream. Nonetheless, LGS2.5D in VATT recovered faster than LGS2.5D in HATT. This occurs due to the high-velocity incoming from the dual disc and it creates high kinetic energy when it reached the LGS turbine and takes a longer time to reach the equilibrium of uniform flow along the downstream. Both VATT and HATT have the fastest recovery in LGS3.5D and despite their similarity in terms of their faster wake recovery, VATT recovered faster than HATT.

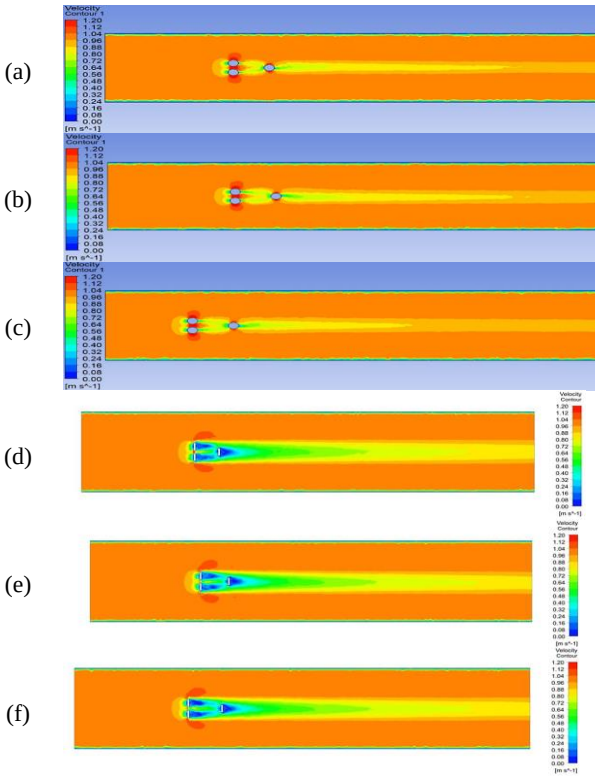

Figure 14: Comparison of velocity contour of dual-frontal staggered arrays between VATT and HATT in LS0.5D: (a) LGS2.5D-VATT (b) LGS3.0D-VATT (c) LGS3.5D-VATT (d) LGS2.5D-HATT (e) LGS3.0D-HATT (f) LGS3.5D-HATT

The next validation is for lateral spacing of 1.0D between VATT and HATT. Both VATT and HATT show a promising result in the velocity contour as illustrated in Figure 15, as there is lesser turbulence mixing occurring at the near wake region and fluid flow that merged at LGS2.5D begins to separate orderly. As the longitudinal spacing increases from 2.5D to 3.0 and 3.5D, the wake recovered faster than longitudinal spacing in LS0.5D. Again, by observing the results between VATT and HATT, it can be observed that VATT recovered faster than HATT. Notably, by analyzing the velocity color region, it is evidenced that there is higher turbulence mixing which is in the green color region at HATT result when compared to VATT. Hence, this indicates that HATT takes longer to develop the steady-state flow across the downstream compared to VATT despite both showing less turbulence mixing as the lateral spacing increase from 0.5D to 1.0D.

As the lateral spacing is increased to 1.5D, the results show a greater wake recovery in comparison to LS1.0D. As shown in Figure 16, the merging flow that separated orderly in LS1.0D is now fully separated into its own individual flow after passing the cylinders and the disc shape turbine. This signifies that there is less turbulence mixing occurs as compared to LS0.5D and LS1.0D. The low kinetic energy from the fluid flow dissipates gradually and causes faster wake recovery at the far wake region. Based on the comparison made between VATT and HATT, it can be said that LS1.5D with LGS3.5D for VATT is more favourable compared to HATT. Hence, another array configuration for single-frontal needs to be done to carry on with the investigation of finding the best array configurations for VATT.

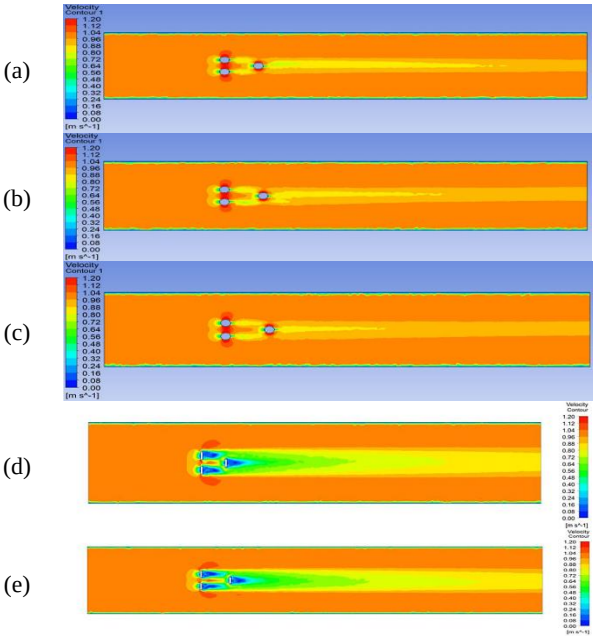

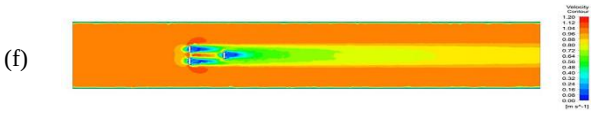

Figure 15: Comparison of velocity contour of dual-frontal staggered arrays between VATT and HATT in LS1.0D: (a) LGS2.5D VATT (b) LGS3.0D VATT, (c) LGS3.5D VATT (d) LGS2.5D HATT, (e) LGS3.0D HATT, (f) LGS3.5D HATT

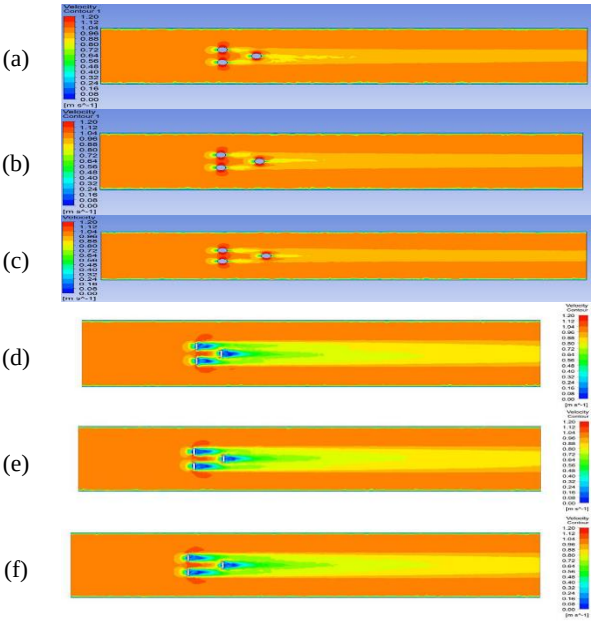

Figure 16: Comparison of velocity contour of dual-frontal staggered arrays between VATT and HATT in LS1.5D: (a) LGS2.5D-VATT (b) LGS3.0D-VATT (c) LGS3.5D-VATT (d) LGS2.5D-HATT (e) LGS3.0D-HATT (f) LGS3.5D-HATT

Validation of Normalized Velocity for Dual-Frontal Staggered Array

Another validation method being used to determine the best array configuration is by calculating the deviation in percentage error of normalized velocity between numerical result and experimental as performed in the single and dual turbine. The first validation is between VATT numerical results and experimental data. As presented in Figure 17, the normalized velocity of VATT has a wide gap with experimental at 5D and 7D downstream. Note that due to space constraints, full plots for Figure 17 and Figure 18 can be found in Appendix A – Figures A1 and A2 respectively. From this figure, it shows that the normalized velocity at these downstream is very poor for the VATT application, especially at the arrangement of the turbines with LGS2.5D and LGS3.0D.

For lateral spacing of 1.0D, Figure 18 shows the deviation between VATT and the experimental has a very poor result across the 5D, 7D and 9D in terms of the normalized velocity. Even though the longitudinal spacing is increasing from LGS2.5D to LGS3.5D, the deviation is still far away from the actual result. One

thing that can be observed is that every single longitudinal spacing, each of them across the far wake region at 25D downstream has less or low deviation error with the actual result. The next validation is between HATT numerical results and experimental data as shown in Figure 18. The numerical result for the normalized velocity shows that as the longitudinal spacing increase, the deviation between the experimental is decreased as well. As illustrated in the plots, the gap between the HATT and experimental is getting smaller across the far wake. This occurs due to high-velocity starting to deficit gradually along the downstream.

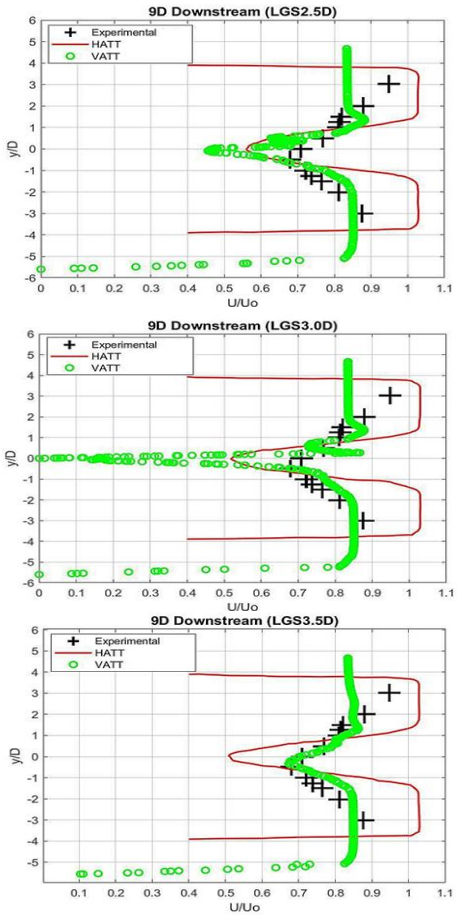

Figure 17: Comparison of normalized velocity between VATT, HATT and experimental in LGS3.0D.

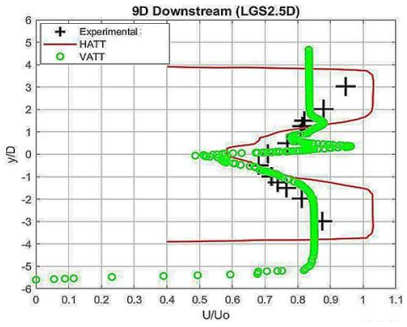

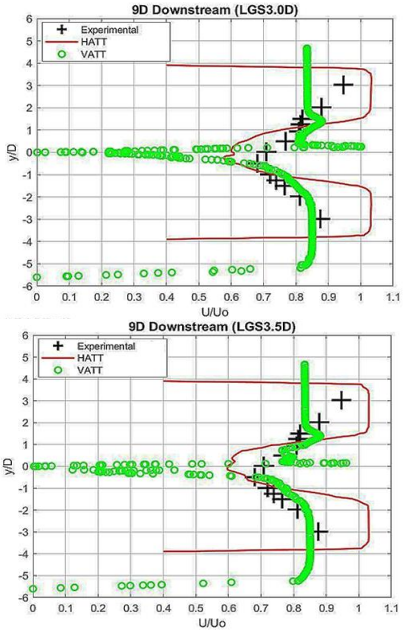

Figure 18: Comparison of normalized velocity between VATT, HATT and experimental in LS1.0D at LGS2.5D, LGS3.0D, and LGS3.5D.

Referring to Table **9**, normalized velocity results for LS0.5D demonstrate a higher deviation percentage of error, mostly at 5D downstream. Notably, LGS2.5D, LGS3.0D and LGS3.5D also have a deviation of more than 50% error. Thus, the best result having a small percentage error for LS0.5D is at LGS3.5D across the 9D and 25D downstream, with both having only 1.43% and 9.64% error respectively against the experimental data. Meanwhile, the deviation between HATT and experimental is small and the gap between the line and the '+' symbol is not separated far between each other. In Table **10**, it is highlighted that the largest HATT high deviation occurs only at LGS2.5D with 37.5% error and a small deviation at LGS2.5D with only 7.23% error. Thus, for HATT and experimental, the best result that having less deviation for LS0.5D is at LGS2.5D across the 25D downstream.

Table 9: Percentage of deviation data between VATT and experimental in LS0.5D

Dual-Frontal Arrays	**Vertical Tidal Turbine VS Experimental** Downstream Distances			
Spacing	5D	7D	9D	25D
LGS 2.5D	66.67%	83.05%	35.71%	16.00%
LGS 3.0D	108.32%	62.71%	44.29%	21.69%
LGS 3.5D	158.33%	15.25%	1.43%	9.64%

Table 10: Percentage of deviation data between HATT and experimental in LS0.5D

Dual-Frontal Arrays	**Vertical Tidal Turbine VS Experimental** Downstream Distances			
Spacing	5D	7D	9D	25D
LGS 2.5D	37.50%	20.34%	18.57%	7.23%
LGS 3.0D	4.17%	28.81%	27.14%	10.84%
LGS 3.5D	20.83%	30.51%	27.03%	9.50%

Lateral spacing 1.0D for VATT shows that the deviation error in LGS2.5D, LGS3.0D and LGS3.5D is 8.54%, 8.43% and 6.10% respectively as shown in Table 11. From the trend, it can be said that the best numerical result for VATT is at the arrangement of LGS3.5D which only shows a 6.10% error. Deviation for all three different longitudinal spacing for HATT (LGS2.5D, LGS3.0D, LGS3.5D) in Table 12 across the 25D downstream shows very good agreement with only 3.66%, 4.88% and 2.44% error respectively. Hence, for HATT with LS1.0D, the best result is represented by using LGS3.5D across the 25D downstream with only 2.44%.

Table 11: Percentage of deviation data between VATT and experimental in LS1.0D

Dual-Frontal Arrays	**Vertical Tidal Turbine VS Experimental** Downstream Distance			
Spacing	5D	7D	9D	25D
LGS 2.5D	129.20%	39.66%	16.90%	8.54%
LGS 3.0D	191.67%	100.00%	43.66%	8.43%
LGS 3.5D	233.33%	82.76%	57.75%	6.10%

Table 12: Percentage of deviation data between HATT and experimental in LS1.0D

Dual-Frontal Arrays	**Vertical Tidal Turbine VS Experimental** Downstream Distance			
Spacing	5D	7D	9D	25D
LGS 2.5D	41.67%	13.79%	18.31%	3.66%
LGS 3.0D	4.17%	17.24%	15.49%	4.88%
LGS 3.5D	62.50%	10.34%	15.35%	2.44%

The final lateral spacing which is LS1.5D shows a similar trend of results in terms of the deviation between numerical results and experimental data. The deviation is higher at the near downstream and then will become lower when it reached the far wake region. As illustrated in Figure 19, the gap between the VATT and experimental in terms of normalized velocity is wider than each other. Note that due to space constraints, full plots for Figure 19 can be found in Appendix A – Figure A3. This indicates that there is no homogeneity between the numerical result for VATT with the experimental. Despite the large deviation at 5D, 7D, and 9D, the result starts to demonstrate an auspicious output at 25D downstream as depicted in Figure 19 similar to the arrangement in LS0.5D and LS1.0D.

Meanwhile, for HATT, the deviation of all the numerical data across the downstream is much more promising compared to VATT. The numerical result shows less deviation and the gap with the experimental is closer to each other. As the longitudinal spacing increase from 5D to 25D, the deviation error starts to reduce gradually, and this obeys the definition of the far wake region. It is observed that, as the downstream distance increases, the faster the wake recovery will be due to the slowing down of the velocity across the domain. But this definition also can be influenced by the lateral spacing and the longitudinal spacing of the array configuration of the turbines.

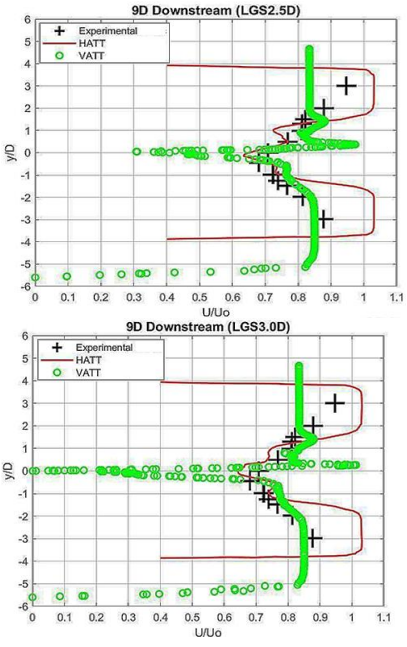

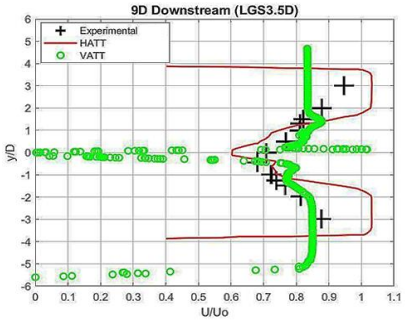

Figure 19: Comparison of normalized velocity between VATT, HATT and experimental in LS1.5D at LGS2.5D, LGS3.0D, LGS3.5D.

The deviation result for VATT in LGS2.5D, LGS3.0D and LGS3.5D across 25D downstream is shown in Table **13** with only 7.41%, 6.17% and 3.70% errors respectively. Again, in VATT the most favorable result will be in the arrangement of LGS3.5D across the 25D downstream. As calculated in Table 14, the reduction of the normalized velocity for HATT at LGS2.5, LGS3.0D and LGS3.5D shows a favorable result. This occurs due to the increase of the lateral spacing from LS1.0D to LS1.5D that causes the velocity to become steady as it across the whole domain. The best result by comparing three different longitudinal spacing for HATT, the optimistic result would be at LGS3.5D across 25D downstream with only 2.46% error.

Table 13: Percentage of deviation data between VATT and experimental in LS1.5D

Dual-Frontal Arrays	**Vertical Tidal Turbine VS Experimental** Downstream Distances			
Spacing	5D	7D	9D	25D
LGS 2.5D	120.83%	83.05%	57.75%	7.41%
LGS 3.0D	195.83%	64.41%	71.83%	6.17%
LGS 3.5D	233.33%	13.56%	73.24%	3.70%

Table 14: Percentage of deviation data between HATT and experimental in LS1.5D

Dual-Frontal Arrays	**Vertical Tidal Turbine VS Experimental** Downstream Distances			
Spacing	5D	7D	9D	25D
LGS 2.5D	66.67%	1.69%	12.68%	1.23%
LGS 3.0D	4.17%	6.78%	8.45%	1.22%
LGS 3.5D	62.50%	18.64%	15.49%	1.24%

Validation Between HATT and VATT for Array Configurations (Single-Frontal Staggered Array)

The idea of single-frontal staggered arrays was proposed by Scott Draper et al [16] and the main purpose of the single-frontal is to explore the behaviour of array configuration and whether it will produce minimal impact on the surrounding or vice versa. The origin of idea by Scott Draper was to locate the second row of the tidal turbine at the side of the domain. The limitation of spacing in Malaysia's coastline that involve various activities such as scuba diving, fish farming, shipping and logistic, and some local boat activities caused the layout to be modified into a smaller region to minimize the effect of tidal turbine layout on the surrounding. Figure 20 shows the comparison of velocity contour at a lateral spacing of 0.5D between VATT and HATT. It can be observed that both of the results demonstrate a poor outcome because they are both experiencing high turbulence mixing that occurs at the second-row turbines.

However, for VATT, the results are slightly better since the model only demonstrates small turbulence occurrence due to low kinetic energy at the back section of the second-row turbines. This could be due to the energy from the flow is already dispersed around the curvy shape of the cylinder turbine. The similarity between these two different turbines is the presence of merging flow at second-row turbines that is caused by the smaller lateral spacing between the cylinder that led to the increase of velocity when it is passing through a small section. Additionally, the presence of turbulence mixing that occurs in the green contour colour indicates the velocity transition from high to low as it is passing the single-frontal cylinder.

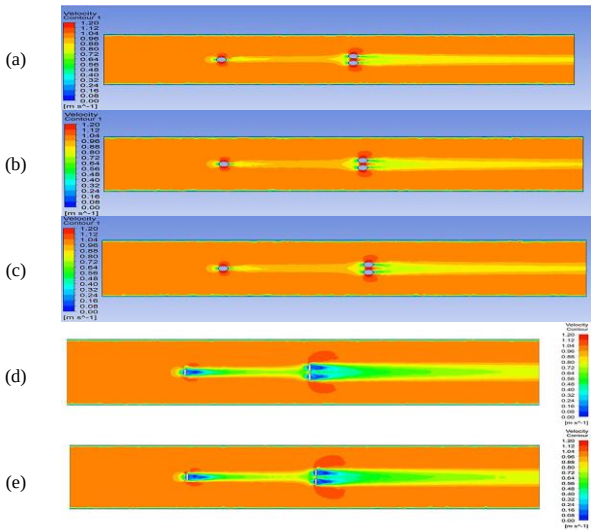

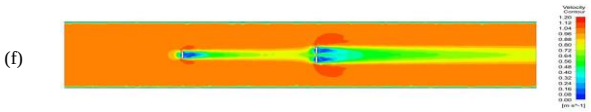

Figure 20: Comparison of velocity contour of single-frontal staggered arrays between VATT and HATT in LS0.5D. (a) LGS13.0D-VATT, (b) LGS13.5D-VATT, (c) LGS14.0D-VATT, (d) LGS13.0D-HATT, (e) LGS13.5D-HATT, (f) LGS14.0D-HATT

Next Figure 21 illustrates the velocity contour between VATT and HATT in the lateral spacing of 1.0D. The major difference that can be identified from the results is that the flow starts to separate midway as it passes through the second-row turbines. The gradual separation begins with the increase of distance in longitudinal spacing. The green region as shown in Figure 21 illustrates the transition region for the velocity of the fluid and the green region takes a longer time to become steady across the downstream distances. In comparison, the results for VATT shows a smaller green contour transition region at the turbulence mixing region. This indicates that, for lateral spacing 1.0D, VATT recovers faster than HATT due to the low kinetic energy that passes through the dual turbines.

Final validation of single-frontal for VATT and HATT in the lateral spacing of 1.5D is done a bit differently compared to the others two lateral spacing. For lateral spacing 1.5D, the longitudinal spacing was changed to 4 different distances which is LGS3.0D, LGS8.0D, LGS10.0D, and LGS13.0D. Significantly, both results produced in VATT and HATT show faster wake recovery compared to previous lateral spacing. This can be observed by referring to Figure 22, where the wake recovery region at the green contour is separated away by each individual flow at the second-row turbines. The factor that leads to this fast wake recovery is the larger spacing between the dual turbines that creates low kinetic energy of the fluid thus it created less turbulence mixing at the near wake. For HATT as done by Hoe [6], it was stated that the most favourable result for the single-frontal array is at LS1.5D in LGS8.0D and for VATT, the most outstanding result is at LS1.5D in LGS13.0D.

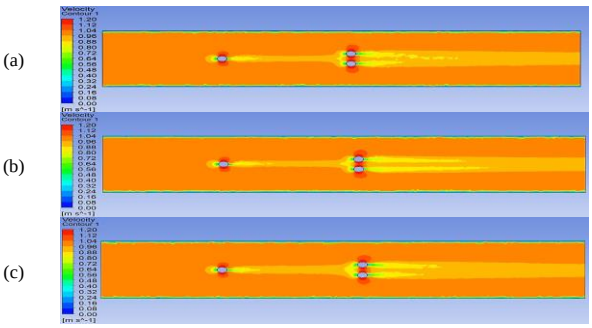

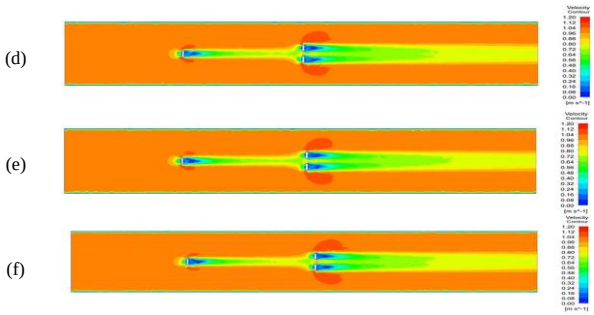

Figure 21: Comparison of velocity contour of single-frontal staggered arrays between VATT and HATT in LS1.0D. (a) LGS12.5D-VATT, (b) LGS13.0D-VATT, (c) LGS13.5D-VATT, (d) LGS12.5D-HATT, (e) LGS13.0D-HATT, (f) LGS13.5D-HATT

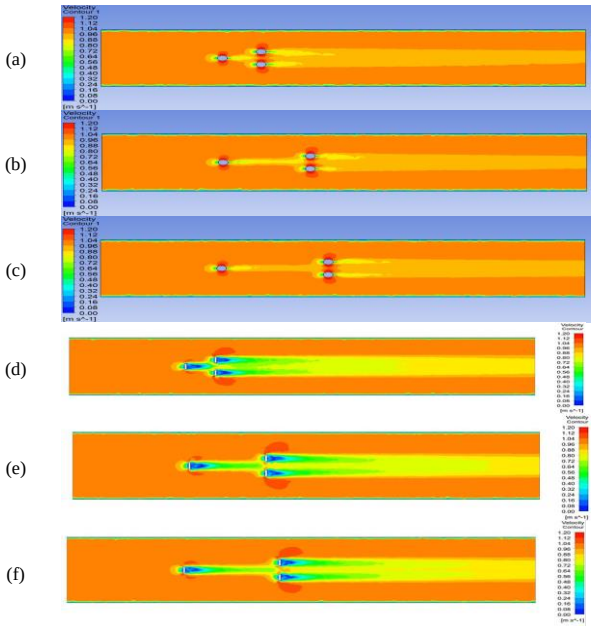

Figure 22: Comparison of velocity contour of single-frontal staggered arrays between VATT and HATT in LS1.5D. (a) LGS3.0D-VATT, (b) LGS8.0D-VATT, (c) LGS10.0D-VATT, (d) LGS3.0D-HATT, (e) LGS8.0D-HATT, (f) LGS10.0D-HATT

CONCLUSION

To conclude, based on the results presented, VATT is preferable to HATT for a single turbine model. Less turbulence mixing and faster wake recovery have led to the choices of VATT compared to HATT. The deviation percentage of VATT and HATT showed small error differences upon comparison with the experimental data. A possible reason for the deviation observed could be due to the meshing setup. For dual turbine simulation, the arrangement of lateral spacing 1.5D in VATT shows more promising results compared to HATT. Although both turbine models had faster wake recovery across the different lateral spacing, the rate of

recovery in VATT was way faster and demonstrated the least deviation in results against experimental data. Additionally, lower kinetic energy from the fluid flow was observed as the lateral spacing increased. Consequently, the wake would recover to the ambiance velocity faster and reach the equilibrium state of the fluid flow.

Meanwhile, for array configuration in dual-frontal staggered arrays, HATT showed more promising results when compared to VATT. Notably, there are two options for choosing the optimal turbine design. If the evaluation is made only by only referring to the velocity contour, then VATT would be the best choice for a dual-frontal staggered array because the generated wake for VATT at any lateral spacing showed quicker recovery compared to HATT. In contrast, evaluation can also be made by referring to the normalized velocity and turbulence intensity of VATT and HATT. The plotting of normalized velocity illustrated that the HATT data was closer to the experimental values, indicating small a percentage error. However, this is to be expected since the experimental data was extracted from a study that employed a horizontal axis turbine. Hence, based on the results and analysis presented, VATT would be the best option to be used in shallow water conditions.

ACKNOWLEDGMENTS

The authors gratefully acknowledge the support received from the Ministry of Higher Education Malaysia through the Fundamental Research Grant Scheme for Research Acculturation of Early Career Researchers (FRGSRACER) RACER/1/2019/ TK07/ UNIMAP/1. Additionally, the authors are also thankful for the support received from Universiti Malaysia Perlis, specifically from the Research Management Centre (RMC).

REFERENCES

[1] K. A. Rahim and A. Liwan, "Oil and gas trends and implications in Malaysia," *Energy Policy*, vol. 50. pp. 262–271, 2012.

[2] U.S Energy Information Administration, "Country Analysis Brief: Malaysia," *Eia*, pp. 1–20, 2017.

[3] H. W. Liu, S. Ma, W. Li, H. G. Gu, Y. G. Lin, and X. J. Sun, "A review on the development of tidal current energy in China," *Renew. Sustain. Energy Rev.*, vol. 15, no. 2, pp. 1141–1146, 2011.

[4] I. Tide, T. Range, and T. Power, "Learn more about Tidal Current Prefeasibility Assessment of a Tidal Energy System Near-Surface Sediment," 2019.

[5] E. W. Purnomo and D. P. Ghosh, "Identifying shallow water flow in offshore Malaysia using multicomponent data and FWI approach," *Offshore Technol. Conf. Asia 2018, OTCA 2018*, no. July, 2018.

[6] B. C. Hoe, "THE INFLUENCE OF TIDAL TURBINES IN ARRAY CONFIGURATION ON THE WAKE FORMATION FOR SHALLOW WATER School of Mechatronic Engineering," no. 161110607, 2019.

[7] K. N. A. M. Shahirah Hayati Mohd Salleh, Anizawati Ahmad, Wan Hanna Melini Wan Mohtar, Chai Heng Lim, "Effect of projected sea level rise on the hydrodynamic and suspended sediment concentration profile of tropical estuary," *Reg. Stud. Mar. Sci.*, vol. 225–236, 2018.

[8] M. H. Baba-Ahmadi and P. Dong, "Numerical simulations of wake characteristics of a horizontal axis tidal stream turbine using actuator line model," *Renewable Energy*, vol. 113. pp. 669–678, 2017.

[9] B. Johnson, J. Francis, J. Howe, and J. Whitty, "Computational Actuator Disc Models for Wind and Tidal Applications," *J. Renew. Energy*, 2014.

[10] H. T. H. Le, C. C. Nguyen, and T. H. Luong, "Performance prediction of Darrieus vertical axis wind turbines using double multiple stream-tube model," *Sci. Technol. Dev. J.*, vol. 18, no. 4, pp. 153–161, 2015.

[11] C. R. Vogel, R. H. J. Willden, and G. T. Houlsby, "Blade element momentum theory for a tidal turbine," *Ocean Engineering*, vol. 169. pp. 215–226, 2018.

[12] P. Bachant, A. Goude, and M. Wosnik, "Actuator line modeling of vertical-axis turbines," no. September, 2016.

[13] A. AbdelSalam, M. Abuhegazy, I. Sakr, and W. El-Askary, "The Impact of Different Inflow Conditions on the Wake of Horizontal Axis Wind Turbine," *J. Eng. Sci. Mil. Technol.*, vol. 17, no. 17, pp. 1–14, 2018.

[14] A. Abolghasemi, M. D. Piggott, and J. Spinneken, "Simulating tidal turbines with mesh optimisation and RANS turbulence models," *Proc. 11th Eur. Wave Tidal Energy Conf.*, no. April 2017, pp. 1–10, 2015.

[15] M. E. Harrison, W. M. J. Batten, L. E. Myers, and A. S. Bahaj, "Comparison between CFD simulations and experiments for predicting the far wake of horizontal axis tidal turbines," *IET Renew. Power Gener.*, vol. 4, no. 6, pp. 613–627, 2010.

[16] T. A. A. Adcock, S. Draper, and T. Nishino, "Tidal power generation - A review of hydrodynamic modelling," *Proc. Inst. Mech. Eng. Part A J. Power Energy*, vol. 229, no. 7, pp. 755–771, 2015.

APPENDIX A

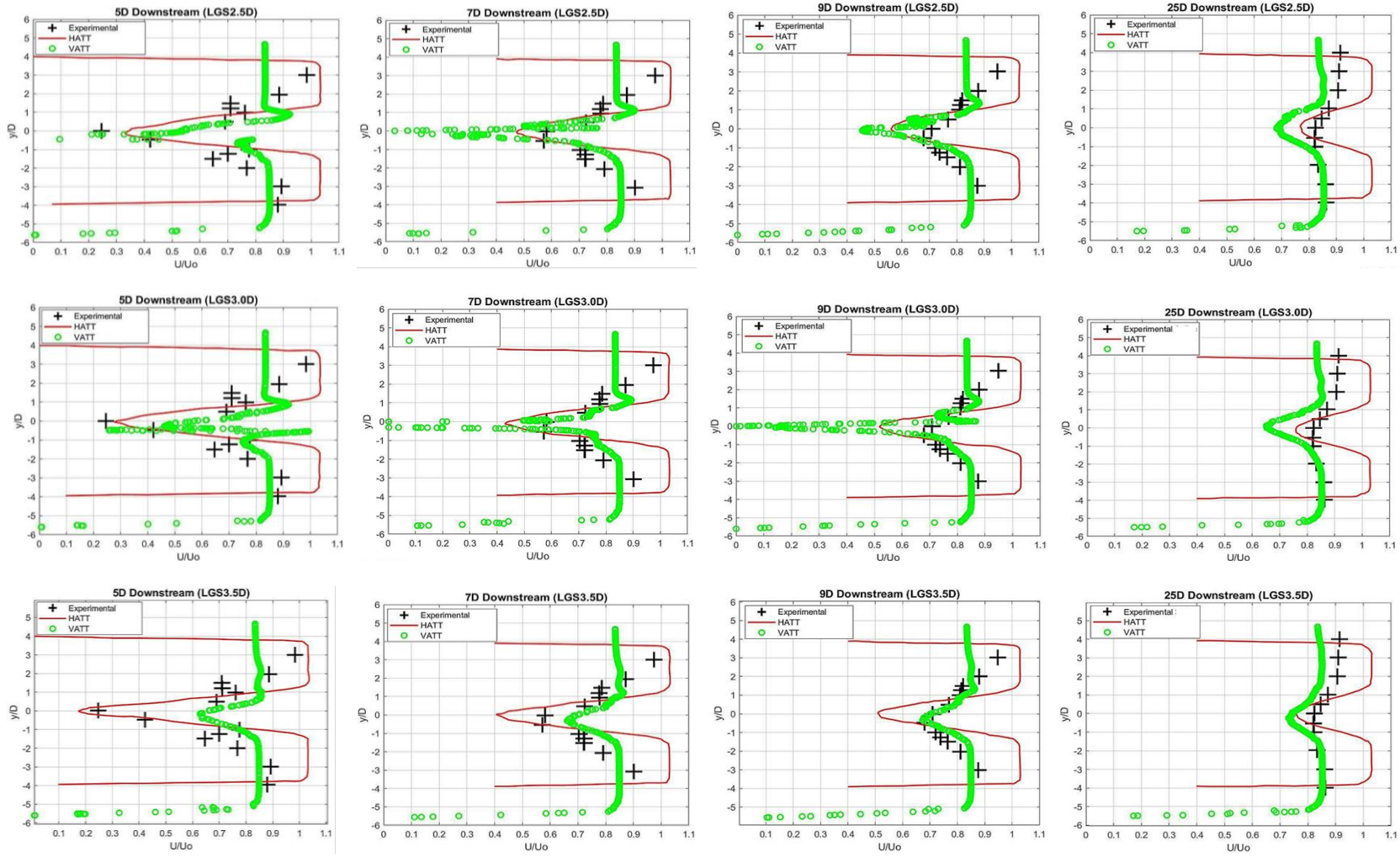

Figure A1: Comparison of normalized velocity between VATT, HATT and experimental in LS0.5D at LGS2.5D, LGS3.0D, LGS3.5D.

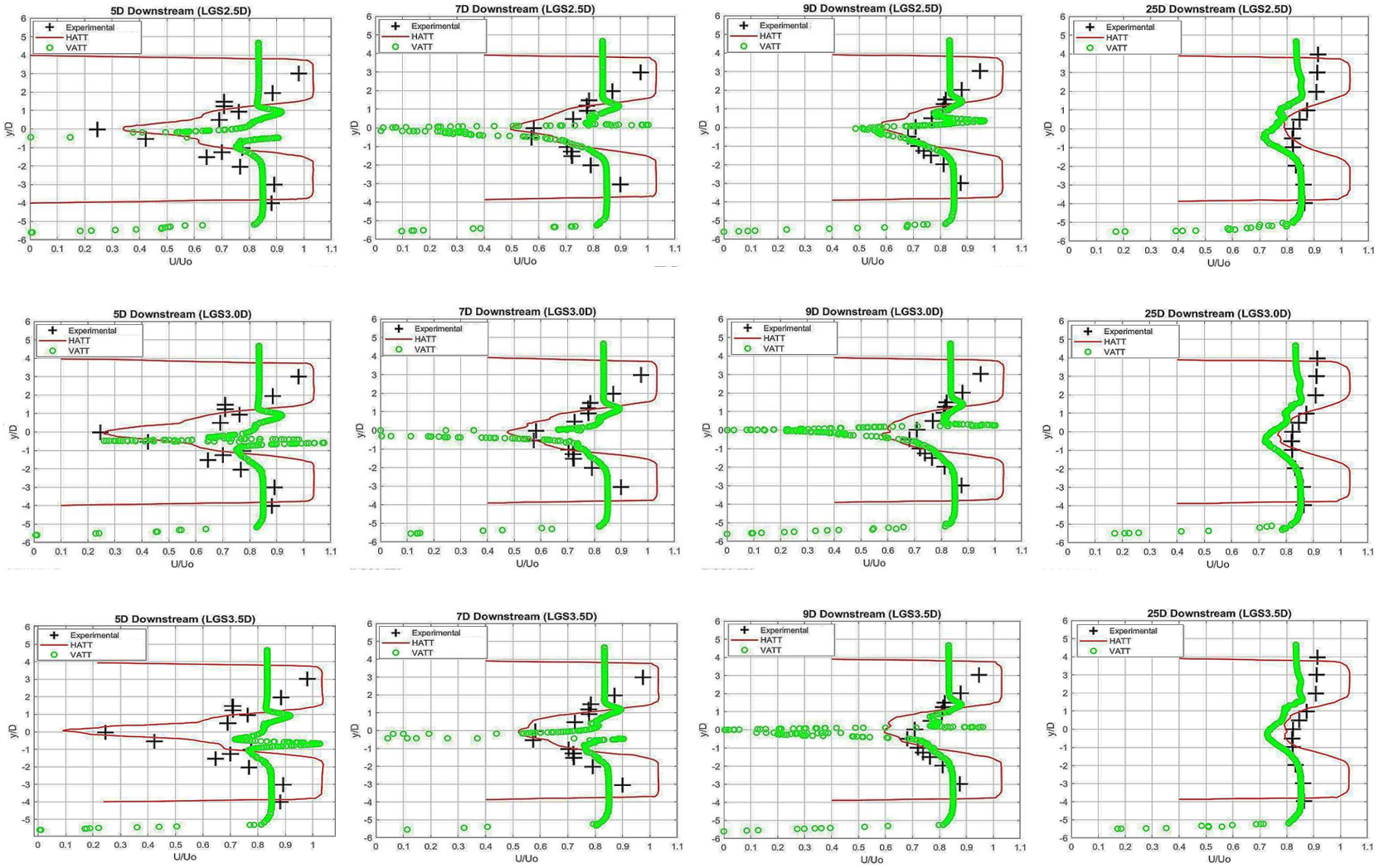

Figure A2: Comparison of normalized velocity between VATT, HATT and experimental in LS1.0D at LGS2.5D, LGS3.0D, LGS3.5D.

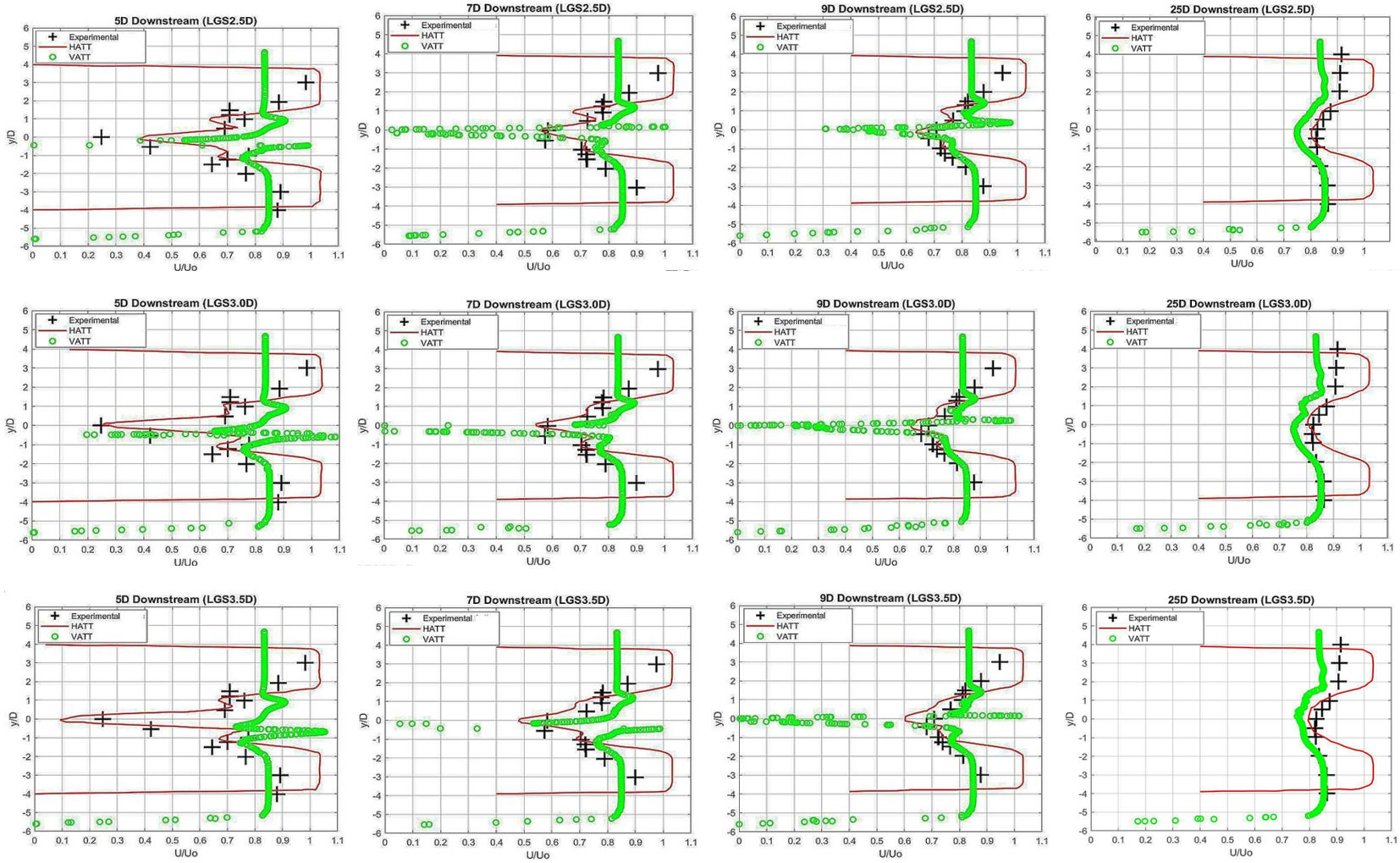

Figure A3: Comparison of normalized velocity between VATT, HATT and experimental in LS1.5D at LGS2.5D, LGS3.0D, LGS3.5D.